Accepted to *The Astrophysical Journal* 12/09/2007
Preprint typeset using LaTeX style emulateapj v. 05/04/06

LARGE-SCALE ANISOTROPIC CORRELATION FUNCTION OF SDSS LUMINOUS RED GALAXIES

Teppei Okumura[1], Takahiko Matsubara[1], Daniel J. Eisenstein[2], Issha Kayo[1], Chiaki Hikage[1,3], Alexander S. Szalay[4], & Donald P. Schneider[5]

Accepted to The Astrophysical Journal 12/09/2007

ABSTRACT

We study the large-scale anisotropic two-point correlation function using 46,760 luminous red galaxies at redshifts 0.16 – 0.47 from the Sloan Digital Sky Survey. We measure the correlation function as a function of separations parallel and perpendicular to the line of sight in order to take account of anisotropy of the large-scale structure in redshift space. We find a slight signal of baryonic features in the anisotropic correlation function, i.e., a "baryon ridge" corresponding to a baryon acoustic peak in the spherically averaged correlation function which has already been reported using the same sample. The baryon ridge has primarily a spherical structure with a known radius in comoving coordinates. It enables us to divide the redshift distortion effects into dynamical and geometrical components and provides further constraints on cosmological parameters, including the dark energy equation-of-state. With an assumption of a flat Λ cosmology, we find the best-fit values of $\Omega_m = 0.218^{+0.047}_{-0.037}$ and $\Omega_b = 0.047^{+0.016}_{-0.016}$ (68% CL) when we use the overall shape of the anisotropic correlation function of $40 < s < 200\ h^{-1}$ Mpc including a scale of baryon acoustic oscillations. When an additional assumption of $\Omega_b h^2 = 0.024$ is adopted, we obtain $\Omega_{\rm DE} = 0.770^{+0.051}_{-0.040}$ and $w = -0.93^{+0.45}_{-0.35}$. These constraints are estimated only from our data of the anisotropic correlation function, and they agree quite well with values both from the cosmic microwave background (CMB) anisotropies and from other complementary statistics using the LRG sample. With the CMB prior from the 3 year *WMAP* results, we give stronger constraints on those parameters.

Subject headings: cosmological parameters — cosmology: observations — galaxies: distances and redshifts — large-scale structure of universe — methods: statistical

1. INTRODUCTION

Recently, baryon acoustic oscillations have been observed in the large-scale structure of the universe. These observations include an analysis of the two-point correlation function (2PCF) of the Sloan Digital Sky Survey (SDSS) Luminous Red Galaxy (LRG) spectroscopic sample (Eisenstein et al. 2005, E05, hereafter), the power spectrum of the Two-Degree Field (2dF) Galaxy Redshift Survey (Cole et al. 2005) and the SDSS LRG (Hütsi 2006a,b; Tegmark et al. 2006; Percival et al. 2007a,b), and the angular power spectrum of the SDSS LRG sample with photometric redshifts (Padmanabhan et al. 2007; Blake et al. 2006). There is a hint of acoustic oscillations in the SDSS quasar sample (Yahata et al. 2005). These analyses have established the ability of the baryon acoustic oscillations to constrain cosmological parameters competitively and complementarily with the CMB (e.g., Spergel et al. 2007) and Type Ia supernovae (Riess et al. 1998; Perlmutter et al. 1999).

These previous analyses of the baryon oscillations, however, use angle-averaged 2PCFs, $\xi(s)$, or angle-averaged power spectra, $P(k)$, where s and k are the separation and wavenumber in redshift space, respectively. A certain amount of information is lost when anisotropies of structure are ignored. In their pioneering work, Alcock & Paczyński (1979) proposed that geometrical anisotropies in redshift space of the high-z universe can be used as a probe of the cosmological constant. Matsubara & Suto (1996) and Ballinger et al. (1996) pointed out that the anisotropy of the 2PCF and the power spectrum in redshift surveys can constrain the dark energy components. Recently, methods which directly use anisotropy of the baryon acoustic oscillations have been theoretically developed for both the power spectrum (Hu & Haiman 2003; Seo & Eisenstein 2003; Glazebrook & Blake 2005; Seo & Eisenstein 2007) and the 2PCF (Matsubara 2004). These approaches use functions of two variables: separations parallel and perpendicular to the line of sight. Observationally, estimations of such two-variable functions are noisier than one-variable functions. The baryon acoustic signature in the large-scale structure is weak even in one-variable statistics when presently available samples of galaxies are used (see, e.g., E05). Therefore, methods that directly treat the anisotropy of the baryon acoustic feature require very large survey volume (Eisenstein et al. 1999; Matsubara & Szalay 2001). Peacock et al. (2001) and Hawkins et al. (2003) measured the 2PCF with two variables from the 2dFGRS (Colless et al. 2001) and detected the detailed signature of large-scale coherent infall, and as a result were able to constrain a value of $\beta \simeq \Omega_m^{0.6}/b$ which parameterizes linear redshift distortions. However, they used information from scales much smaller than the acoustic scale because of limited survey

Electronic address: teppei@a.phys.nagoya-u.ac.jp
[1] Department of Physics, Nagoya University, Chikusa, Nagoya, 464–8602, Japan
[2] Steward Observatory, University of Arizona, 933 N. Cherry Ave., Tucson, AZ 85121
[3] School of Physics and Astronomy, University of Nottingham, University Park, Nottingham, NG7 2RD, UK
[4] Department of Physics and Astronomy, The Johns Hopkins University, Baltimore, MD 21218
[5] Department of Astronomy and Astrophysics, Pennsylvania State University, University Park, PA 16802

volume and did not analyze the effect of geometrical distortion. On the other hand, the correlation analyses of the 2dF QSO survey placed constraints on the cosmological constant (Hoyle et al. 2002; Outram et al. 2004; da Ângela et al. 2005; see also Ross et al. 2007). Their analyses still focused on smaller scales than the baryon acoustic scale.

In this paper we analyze the anisotropic 2PCF, including the baryon acoustic peak in the large-scale structure and constrain relevant cosmological parameters. We use a spectroscopic sample of the SDSS LRG, which is the most useful sample for our purpose. Our analysis differs from previous studies of baryon acoustic oscillations in the LRG sample in that, owing to a theoretical development by Matsubara (2004), we take into consideration the fully two-dimensional feature in the 2PCF to detect a geometrical distortion effect; this is the first cosmological application of the two-dimensional acoustic peaks.

Before proceeding to the next section, we take note of nonlinearity on large scales and the scale dependence of the galaxy biasing. The nonlinear effects on the baryonic features that appear around 100 h^{-1} Mpc play an important role in taking account of percent-level cosmology (e.g., Meiksin et al. 1999; Seo & Eisenstein 2005; Jeong & Komatsu 2006). Recent work also suggests that the scale-dependent biasing poses a serious problem in analyzing galaxy surveys (e.g., Blanton et al. 2006; Percival et al. 2007b; Smith et al. 2007; Coles & Erdoğdu 2007; Sánchez & Cole 2008). However, for the sake of simplicity, in this paper we consider only the large-scale clustering and assume the biasing to be scale-independent and linear.

The structure of this paper is as follows. In § 2 we describe the SDSS LRG sample used in our analysis. We then, in § 3, measure the anisotropic 2PCF in redshift space and estimate its covariance matrix. In § 4 we outline the cosmological parameter dependence on the modeled 2PCF, including dynamical and geometrical distortions. Cosmological parameters are constrained by the measured anisotropic 2PCF in § 5. In § 6 our conclusions are given.

2. THE SDSS LRG SAMPLE

The SDSS (York et al. 2000; Stoughton et al. 2002) is an ongoing imaging and redshift survey which uses a dedicated 2.5m telescope, a mosaic CCD camera, and two fiber-fed double spectrographs (Fukugita et al. 1996; Gunn et al. 1998, 2006). After image processing (Lupton et al. 2001; Stoughton et al. 2002; Pier et al. 2003; Ivezić et al. 2004; Tucker et al. 2006) and calibration (Hogg et al. 2001; Smith et al. 2002), the spectroscopic targets of LRGs are selected from the imaging data according to the algorithm described by Eisenstein et al. (2001). The tiling algorithm for the fibers is found in Blanton et al. (2003a).

For our analysis, we use 46,760 LRGs over 3853 deg^2 in the redshift range from 0.16 to 0.47, which is the same sample as the one used in previous analyses of SDSS LRG clustering (Zehavi et al. 2005; E05). The sky coverage is the same as lss_sample14 (Blanton et al. 2005) and is similar to that of the publicly available SDSS Data Release 3 (Abazajian et al. 2004). The galaxies in the sample have rest-frame g-band absolute magnitudes $-23.2 < M_g < -21.2$ ($H_0 = 100$ km s^{-1} Mpc^{-1}) with $K+E$ corrections of passively evolved galaxies to a fiducial redshift of 0.3 (Blanton et al. 2003b). The comoving number density of the sample is close to constant out to $z = 0.36$ (i.e., volume limited) because of the narrow absolute magnitude cut, and drops thereafter due to the flux limits (see Fig. 1 of Zehavi et al. 2005). The radial and angular selection functions, fiber collisions, and unobserved plates are modeled using the method described in Zehavi et al. (2005); E05 also provides the details of the sample.

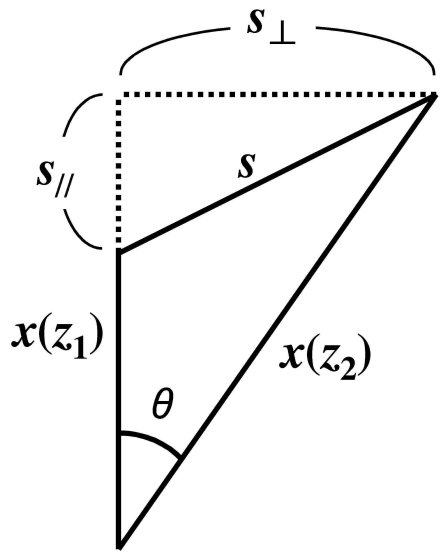

FIG. 1.— Illustration of geometrical quantities used in this paper.

3. ANISOTROPIC 2PCF OF LRGS

3.1. *Measuring the LRG 2PCF*

The 2PCF is measured by comparing the actual galaxy distribution to a catalogue of randomly distributed points in the same region, according to the selection function of the survey (Peebles 1980). We count the galaxy pairs in bins of comoving separation along and across the line of sight, $s_\parallel$ and $s_\perp$ respectively, to estimate the anisotropic 2PCF. Our notations of geometric quantities are illustrated in Figure 1. First, the comoving distances to every galaxy, $x(z)$, are calculated by assuming a flat universe with $\Omega_m = 0.3$ and $\Omega_\Lambda = 0.7$, where Ω_m is the mass density parameter and Ω_Λ is the cosmological constant parameter. This flat universe is used only as a mapping between the observed space and our analysis space: our theoretical modeling also takes this mapping into account. The purpose of the mapping is simply to avoid having to perform the analysis in strongly distorted redshift space. For each galaxy with redshift z_1 we define the separations $s_\parallel$ and $s_\perp$ of other galaxies with redshift z_2 according to Figure 1:

$$s_\parallel = x(z_2)\cos\theta - x(z_1), \quad (1)$$

$$s_\perp = x(z_2)\sin\theta, \quad (2)$$

where θ is the apparent angle between the two galaxies from the observer. This definition of the line of sight is not as standard as that of (r_p, π), such as was defined by Davis & Peebles (1983; see also Fisher et al. 1994).

Which galaxy of the pair is chosen as galaxy 1 is arbitrary in our definition. Both galaxies are considered as

galaxy 1, and the line of sight is simply defined as the direction toward the galaxy 1. Therefore we count a pair of galaxies twice. As a result, there appears a strong correlation between certain bins in $(s_\perp,\ s_\parallel)$ space; in particular, the bins of opposite sign of $s_\parallel$ are strongly correlated. Those bins contain almost identical pairs in a small-angle case, $\theta \ll 1$. However, the angle θ in our sample is not always this small, so that those bins contain different sets of pairs. Still the correlations between those bins are strong, which is properly taken into account in our parameter estimation below.

We compute the anisotropic 2PCF using the Landy-Szalay estimator (Landy & Szalay 1993),

$$\xi(s_\perp,\ s_\parallel) = \frac{DD - 2DR + RR}{RR}, \qquad (3)$$

where DD, RR, and DR are the normalized counts of galaxy-galaxy, random-random, and galaxy-random pairs, respectively, in a particular bin in the space of $(s_\perp,\ s_\parallel)$. The random catalogue contains about 30 times as many points as the real data, and the random points are distributed according to the radial and angular selection functions. The space of $(s_\perp,\ s_\parallel)$ is divided into rectangular cells with $\Delta s_\perp,\ \Delta s_\parallel = 10\ h^{-1}$ Mpc. Each galaxy of redshift z is weighted by $1/[1+n(z)P_w]$, where $n(z)$ is the comoving number density and P_w is the power spectrum at a typical scale (Feldman et al. 1994). We adopt $P_w = 40,000\ h^{-3}$ Mpc^3, which is evaluated at the baryon wiggle scale and is the same value as E05. We have also tried another value, $P_w = 30,000 h^{-3}$Mpc^3, adopted by Tegmark et al. (2006). We found that the value does not have a strong effect on the result, as noted in Percival et al. (2007b), because the comoving number density of our sample is close to constant at almost all scales.

The resulting redshift-space 2PCF for the observed LRGs is shown in the right half of the plane in Figure 2. The value of $\xi(s_\perp,\ s_\parallel)$ are given by contour lines. There is an indication of the baryon ridges of radius about 100 h^{-1} Mpc, which is a counterpart of the baryon peak in the one-dimensional 2PCF, although the signal is not so strong. The anisotropy of the clustering is obvious in this figure. When the separation is along the line of sight $(s_\perp \approx 0)$, the clustering is elongated due to nonlinear velocity dispersions of galaxies. On the other hand, the large-scale clustering is squashed along the line of sight due to coherent infalls toward over-dense regions (Kaiser 1987). The latter effect is often called the Kaiser's effect. A corresponding theoretical prediction based on a linear perturbation theory derived by Matsubara (2000, 2004) is shown in the left half of the plane in Figure 2. Although the measured 2PCF is noisy, the linear theory can account for the behavior of the 2PCF on large scales. The nonlinear velocity distortions are not described by linear dynamics, which should be removed in our linear analysis below. The detailed comparison clearly needs statistical treatment, which we explain below. When the anisotropic 2PCF is averaged over the angle, the one-dimensional 2PCF $\xi(s)$ is obtained.

3.2. *Covariance Matrix*

Because there are strong correlations between different bins of the anisotropic 2PCF, it is necessary for statistically proper analyses to estimate a covariance matrix.

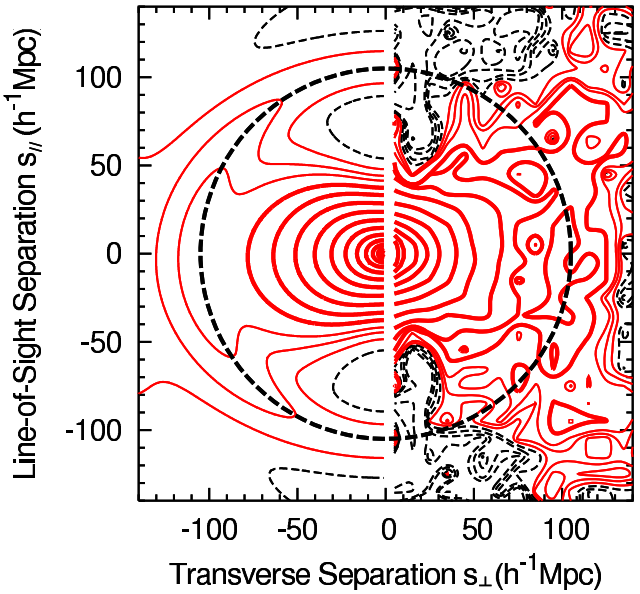

FIG. 2.— Contour plots of the redshift-space 2PCF measured from the SDSS LRG sample (*right*) and the corresponding analytical formula derived by Matsubara (2004) using a linear perturbation theory (*left*). The dashed black lines show $\xi < -0.01$ increasing logarithmically with 0.25 and $-0.01 \le \xi < 0$ linearly with 0.0025. The solid thin lines colored red show $0 \le \xi < 0.01$ increasing linearly with 0.0025 and the solid thick ones colored red $\xi \ge 0.01$ logarithmically with 0.25. The baryonic feature slightly appears as ridge structures around the scale $s = (s_\perp^2 + s_\parallel^2)^{1/2} \simeq 100\ h^{-1}$ Mpc, and the dashed circle traces the peaks of the baryon ridges . For the theoretical predictions, we adopt the best-fit values assuming a flat cosmology, $\Omega_{\rm m} = 0.218$, $\Omega_b = 0.0473$, $h = 0.702$, $\sigma_8 = 0.660$, $b = 1.55$, while the fiducial values, $n_s = 1$ and $w = -1$ are fixed. We also set the redshift at the origin to be 0.34, which is typical in our LRG sample.

For this purpose, jackknife resampling or bootstrap resampling (e.g., see Lupton 1993) is often adopted. In a cosmological context, however, cosmic variance plays a critical role in estimates of cosmological parameters. It is uncertain whether these methods can provide a reliable estimator of the cosmic variance because they rely only on one observed sample. We first tried to use the jackknife method and found that this approach actually underestimates the covariance at all the scales, which leads to the underestimation of the error bars for cosmological parameters when we compare them with a more reliable method explained below. A similar tendency is also seen by Pope & Szapudi (2007).

One of the best ways to estimate the covariance matrix including cosmic variance is to use N-body simulations to generate many mock catalogs from which the covariance matrix is calculated. It is necessary to generate a larger number of mock samples than the number of data points of the statistics to be employed; otherwise, one would improperly obtain a singular covariance matrix. However, because our analysis of the anisotropic 2PCF deals with several hundred data points, it is computationally too expensive to produce a sufficient number of independent realizations in our case.

In our analysis we adopt an alternative method, using a public second-order Lagrangian perturbation theory (2LPT) code (Crocce et al. 2006). As input ingredients, we adopt $\Omega_m = 0.27$, $\Omega_\Lambda = 0.73$, $h = 0.7$, $\sigma_8 = 0.8$, 256^3 particles in a cubic box of side 1600 h^{-1} Mpc, and a transfer function calculated by CMBfast code

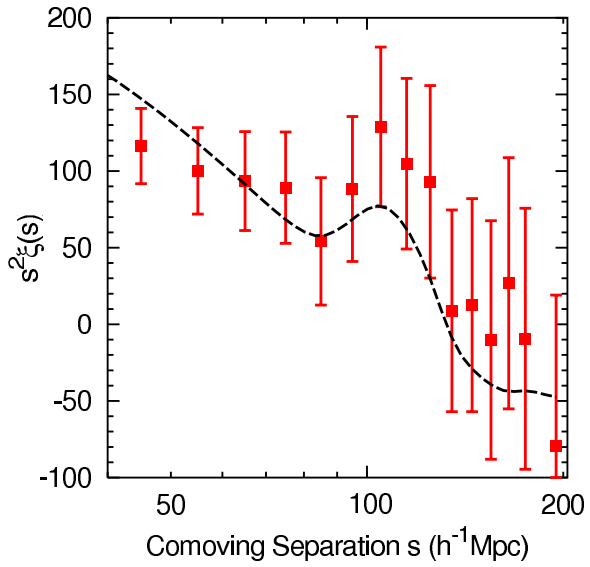

FIG. 3.— Comparison of the 2PCFs times s^2 between the observed LRGs and the mock catalogs. The horizontal axis is logarithmic while the vertical axis is linear. The red points show the angle-averaged 2PCF of the LRGs and the error bars are from the mock catalogs. The dashed line shows the 2PCF averaged over the mock catalogs. The baryon peak detected in these plots is obtained from the integration of baryon ridges in Fig. 2 over angular orientation.

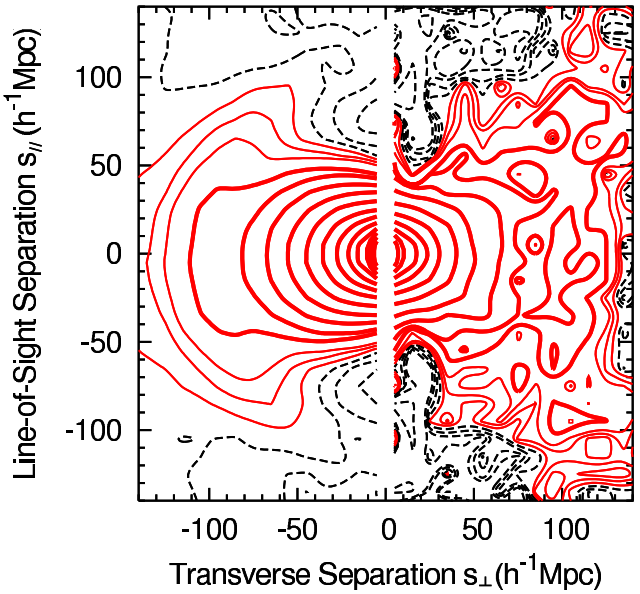

FIG. 4.— Anisotropic 2PCFs as functions of two variables, separations perpendicular and parallel to the line of sight. The right side shows the LRG 2PCF, which is the same as the right one of Fig. 2. The left side shows the corresponding averaged 2PCF of our mock catalogs. The difference between 2PCFs in each mock and their average is used for construction of the covariance matrix. The 2PCF from our mock catalogs does not have large deviation from that of the observed 2PCFs, even for the quadrupole components.

(Seljak & Zaldarriaga 1996) with $\Omega_b = 0.045$, where h is the Hubble parameter normalized by 100 km s^{-1} Mpc^{-1}, σ_8 is the rms. of the fluctuations smoothed with a top-hat window function of radius $R = 8\ h^{-1}$ Mpc, and Ω_b is the baryon density parameter. To implant the galaxy biasing of the LRGs (Zehavi et al. 2005), we empirically select particles with probability proportional to $e^{\alpha\delta_m}$, where δ_m is the mass density fluctuation at a position of each particle calculated by the University of Washington HPCC's public SMOOTH code.[6] We choose $\alpha = 1.5$ so as to match the correlation amplitude of the observed LRGs at scales larger than 40 h^{-1} Mpc. Then we trim the mock catalogs from simulation boxes so as to have the same number density and the same survey volume as the actual LRG sample. Finally, we generate 2500 mock catalogs with independent initial conditions, compute the 2PCF for each, and obtain a covariance matrix by

$$(\mathbf{C})_{ij} \equiv \mathrm{Cov}(\xi_i, \xi_j) = \frac{1}{N-1}\sum_{l=1}^{N}(\xi_i^l - \bar{\xi}_i)(\xi_j^l - \bar{\xi}_j), \quad (4)$$

where $N = 2,500$, ξ_i^l represents the value of the 2PCF of ith bin in lth realization, and $\bar{\xi}_i$ is the mean value of ξ_i^l over realizations. The average of 2PCFs from each mock catalog agrees well with the observation within the 1 σ errors for both one-dimensional (Fig. 3) and two-dimensional analyses (Fig. 4). These mock catalogs are constructed solely to estimate errors of the measured 2PCF of LRGs, so the averaged 2PCF over the catalogs is not used for the following analyses. Increasing α changes the amplitude at the scales around the baryon peak to match the observation, while it causes more discrepancy at the small scales. This tendency is, however, consistent with the theoretical prediction (see Figure 3 in E05).

[6] At http://www-hpcc.astro.washington.edu/tools/smooth.html.

We test the full covariance matrix obtained by the 2LPT method. First, we randomly choose the 2PCFs of 30 realizations out of 2500. We regard each of 30 2PCFs as an observed LRG sample, calculate the χ^2 statistics by the method described in §5, constrain the input cosmological parameters, Ω_m and h, and check how many realizations contain the input values at 68% and 95% confidence level. If the amplitude of covariance is reasonable, 68% of all the contours of 68% confidence levels should contain the input parameters. The reason for using only 30 realizations is that comparing against all the mock catalogs is computationally very expensive; it requires that χ^2 be calculated in seven dimensional parameter space 2500 times. According to our statistics, anisotropic 2PCF $\xi(s_\perp, s_\parallel)$, there are 22 and 28 realizations which contain the inputs at 68% and 95% confidence levels for Ω_m in the total 30 realizations, while there are 17 and 28 for h. We thus conclude that our method of estimating the covariance matrix is reasonable, and can be reliably applied for parameter estimation in §5. Figure 5 shows the result of the test; we choose to present only 15 realizations because displaying all 30 results makes the figure unclear.

4. THEORETICAL PREDICTIONS

As a theoretical prediction for the anisotropic 2PCF, we adopt an analytical formula of Matsubara (2000, 2004) derived in a general situation taking into account the wide-angle effect (Szalay et al. 1998) and the high-z distortion effect (Matsubara & Suto 1996) in linear perturbation theory. The necessary formula is given in Matsubara (2004).

The mean redshift of the LRG sample is about 0.34 and the clustering scale which we probe ranges up to 200 h^{-1} Mpc. The maximum angle between two points

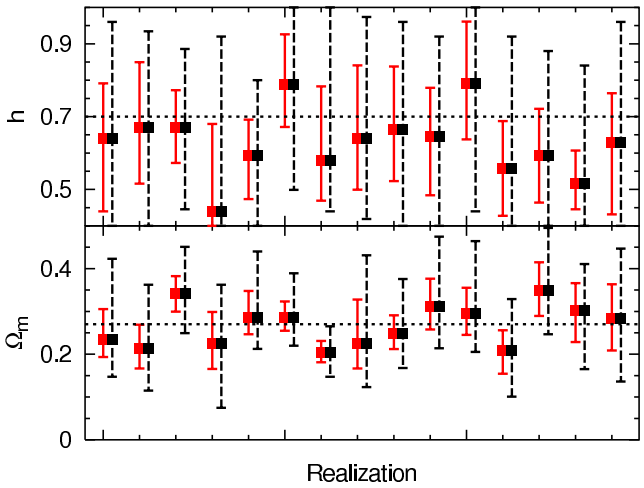

FIG. 5.— Display of the reliability of the recovery of Ω_m and h from 15 realizations. The horizontal axis shows the realization number, while the vertical axis shows the value of Ω_m and h and the horizontal dashed lines show their input parameters. Solid and dashed error bars shows the 68% and 95% confidence levels, respectively. Among these 15 realizations, there are 10 and 11 realizations including input values of Ω_m and h, respectively, at 68% confidence intervals , and 14 and 15 at 95% intervals.

from the observer (θ in Fig. 1) is $\approx 12°$. The distant-observer approximation is not so accurate at $\gtrsim 10°$, and therefore the general formula give above, which accurately includes the wide-angle effect, is preferable for a precise analysis of the LRG sample.

The left side of Figure 2 shows a prediction in linear theory of the two-dimensional 2PCF in redshift space with the central redshift of $z_1 = 0.34$. We adopt a flat cosmology with $\Omega_m = 0.218, \Omega_b = 0.0473, h = 0.702, \sigma_8 = 0.660$, $b = 1.55$, $n_s = 1$, and $w = -1$, where $w = p_{\rm DE}/\rho_{\rm DE}$ is the equation-of-state parameter for the dark energy component and b is the linear bias parameter. The first five values are our best-fit values for the two-dimensional 2PCF of LRGs, as described in the following section, while the last two are the fiducial values.

Throughout this paper we assume a flat cosmology for simplicity. There are seven cosmological parameters in our modeling: Ω_m, h, Ω_b, n_s, w, σ_8, and b. For the details of the dependence of the anisotropic 2PCF on cosmological parameters, see Matsubara (2004). In short, there are three kinds of physical effects. The first one is the shape of the underlying mass power spectrum, which is determined by the Ω_m, Ω_b, h, and n_s. The second one is the dynamical distortion effect which is generated by peculiar velocities of galaxies. Linear, coherent velocities squash the apparent clustering along the line of sight, while nonlinear, random velocities smear the clustering along the same direction (Kaiser 1987; Hamilton 1992). The linear squashing effect depends on the so-called redshift distortion factor, $\beta(z) = f(z)/b(z)$, where $f(z) = d\ln D/d\ln a$ is the logarithmic derivative of the linear growth rate $D(z)$ at redshift z, $a = (1+z)^{-1}$ is the scale factor, and $b(z)$ is the linear bias factor at redshift z. The growth factor depends on Ω_m and w. Since we assume a flat cosmology, the density parameter of dark energy is given by $\Omega_{\rm DE} = 1 - \Omega_m$. However, the parameter dependence on the growth factor is not so useful in parameter estimation, because the overall amplitude of the power spectrum characterized by σ_8 is a free parameter. Since the parameter dependence of nonlinear velocity effect is not analytically given, we do not use the nonlinear regime in the 2PCF. The third effect is the geometric distortion, which depends on the Hubble parameter $H(z)$, and angular diameter distance, $D_A(z)$, and thus depends on Ω_m, and w. The dependence of the geometric distortion on h vanishes in redshift surveys in which distances are measured in units of h^{-1}Mpc. The geometric distortion is useful for constraining the dark-energy parameters, $\Omega_{\rm DE}$ and w. The baryon ridges are isotropic in comoving space and their anisotropy is primarily due to geometric distortion.

Finally, we comment on the galaxy biasing and the evolutionary effect. Because we consider only the linear regime, we assume the biasing to be scale-independent and linear. Although the bias parameter b is completely degenerate with σ_8 in the ordinary one-dimensional 2PCF, the two-dimensional 2PCF is able to solve this degeneracy through the measurement of the redshift distortion parameter, β, which depends on b. We treat b and σ_8 as independent parameters in the following analysis. One could choose β or $b\sigma_8$ as free parameters (which are more closely related to the measurements), instead of b or σ_8. The choice of the independent parameters does not affect the following result.

In this paper we consider the measured 2PCF as a representative of the function at a mean redshift $z_1 = 0.34$. We therefore simply neglect the effects of evolution on clustering and biasing within the sample. Strictly speaking, evolutionary effects are not negligible in very large redshift surveys which have broad range of redshift (e.g., Yamamoto & Suto 1999). For example, the evolution has a significant effect in the SDSS quasar sample (Yahata et al. 2005). In our LRG sample, however, the redshift range is relatively small and the signal-to-noise ratio of the measured 2PCF is not very high. Indeed, the evolutionary effect on the growth factor is about less than 20% from the survey edge to the mean redshift, but the effects on the anisotropic 2PCF and cosmological parameters are negligibly small compared to error levels.

5. CONSTRAINTS ON COSMOLOGICAL MODELS

5.1. *Setup*

In this section we describe methods and results of constraining cosmological parameters by the anisotropic 2PCF of the LRG sample. We measure the goodness of fit, which shows how well assumed cosmological parameters fit a set of observational data, and the measurements are given by the χ^2 statistics, taking into account the full covariance matrix. As described in the previous section, we adopt seven free parameters Ω_m $(= 1 - \Omega_{\rm DE})$, Ω_b, h, n_s, w, σ_8, and b, assuming flatness of the universe.

In comparing observational data with theory, we first compute the theoretical 2PCF as a function of (z_1, z_2, θ) with a given set of parameters. Next we use the fiducial parameters of $\Omega_{\rm m} = 0.3$ and $\Omega_\Lambda = 0.7$ to convert redshifts into comoving distances, which are the same values assumed for measuring the distances of each galaxy in § 3.1. Therefore, we compare the theoretical 2PCF with the observation in the same comoving space and these fiducial parameters do not bias our results of parameter estimations.

The theoretical formula based on the linear perturbation theory does not reproduce nonlinear gravitational effects and nonlinear velocity distortions such as finger-

of-God effects. We therefore discard the observed 2PCF at scales less than 40 h^{-1} Mpc. We also do not use the data along the line-of-sight, namely, $s_\perp < 10\ h^{-1}$ Mpc, because the line-of-sight components of the 2PCF are noisy (Bernstein 1994) and furthermore deviate from Kaiser's formula even on large scales (Scoccimarro 2004). Finally we perform the analysis for the scale range of $40 < s < 200\ h^{-1}$ Mpc. We also adopt a more conservative range $60 < s < 160\ h^{-1}$ Mpc to check the systematic effects beyond the linear theory. The numbers of bins in 2PCF are 574 for $40 < s < 200\ h^{-1}$ Mpc and 330 for $60 < s < 160\ h^{-1}$ Mpc. χ^2 statistics are then calculated as

$$\chi^2(\theta) = \sum_{i,j} \Delta\xi_i(\theta)(\mathbf{C}^{-1})_{ij}\Delta\xi_j(\theta), \quad (5)$$

where θ is a set of cosmological parameters to be constrained, $\Delta\xi_i(\theta)$ denotes the difference between the observed and theoretical 2PCFs in ith bin, and the sum is over the number of bins. The most likely values for the cosmological parameters minimize the equation (5). Finally, the likelihood function for the cosmological parameters, $\mathcal{L}$, is proportional to $\exp(-\chi^2/2)$ with an appropriate normalization factor. Then, for example, the 68% confidence interval becomes the region where $\int \mathcal{L}\ d\theta = 0.68$ in the parameter space.

5.2. σ_8-b *degeneracy*

First, we consider the behavior of the parameters related to the clustering amplitude, σ_8 and b. Figure 6 plots their joint likelihood functions with contours representing 68%, 95% and 99% confidence levels, where $w = -1$ is fixed and we marginalize over the other four parameters Ω_m, Ω_b, h, and n_s. We find $\sigma_8 = 0.66^{+0.289}_{-0.216}$ and $b = 1.55^{+1.42}_{-0.75}$ (68% confidence level) for the fit to $40 < s < 200\ h^{-1}$ Mpc after also marginalizing them over each other. As described in § 4, b and σ_8 are strongly coupled as the amplitude of the 2PCF is proportional to a product $b\sigma_8$. The degeneracy is somewhat alleviated from anisotropy of the 2PCF due to dynamical distortions which are dependent on β. It is still difficult, however, to independently constrain these two parameters without relying on other observations such as CMB, higher order correlation analysis, etc. In this paper we mainly focus on parameter constraints only from the 2PCF and consider the joint analysis with the *Wilkinson Microwave Anisotropy Probe* (*WMAP*) results only in § 5.5.

Therefore, we always marginalize over both σ_8 and b in the following likelihood analysis. This marginalization corresponds to mainly using the shape information in the 2PCF and discarding the amplitude information.

We also note that the physical origins of the parameters b and σ_8 are not fully understood. The value of the bias parameter b depends on unknown details concerning the formation of LRGs, and the value of σ_8 depends on unknown details about the generation of density fluctuations in the primordial universe. There is not any reliable theory which robustly predicts the values of these parameters.

5.3. *Main results*

We next focus on the four fundamental cosmological parameters Ω_m, Ω_b, h, and n_s after marginalizing over

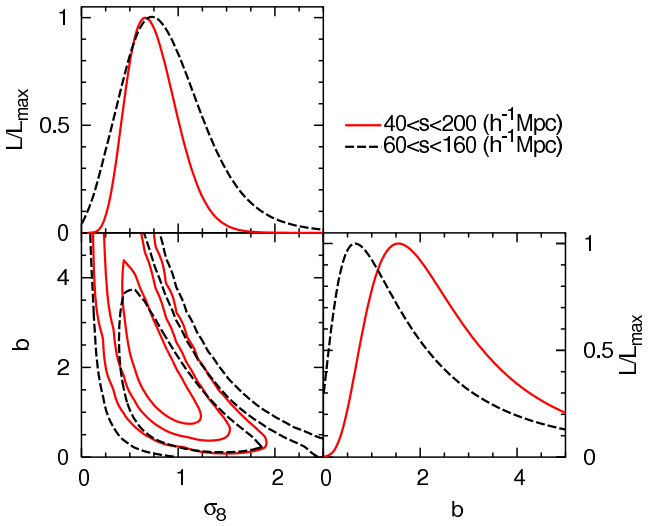

FIG. 6.— Likelihood contours for the parameters related to the clustering amplitude, σ_8 and b. The diagonal panels represent the likelihood functions for the individual parameters, where Ω_m, Ω_b, h, and n_s are marginalized over. The bottom left panel represents a two-parameter constraint, and each ellipse shows the 68%, 95%, and 99% confidence levels from inward. The solid and dashed (colored red and black) contours are the fits for $40 < s < 200\ h^{-1}$ Mpc and $60 < s < 160\ h^{-1}$ Mpc, respectively. The best-fit parameters are $\sigma_8 = 0.66$ and $b = 1.55$ for $40 < s < 200\ h^{-1}$ Mpc.

σ_8 and b. Figure 7 illustrates contour plots of the joint likelihood functions of two parameters among the four, where w is fixed at -1.

The fits to $40 < s < 200\ h^{-1}$ Mpc give $\Omega_m = 0.218^{+0.047}_{-0.037}$, $\Omega_b = 0.0473^{+0.0157}_{-0.0160}$, $h = 0.702^{+0.187}_{-0.117}$, and $n_s = 1.122^{+0.152}_{-0.183}$ (68% CL). The best-fit values and the errors of all the cosmological parameters are listed in Table 1. The best-fit values of all of the four parameters for $40 < s < 200$ and $60 < s < 160\ h^{-1}$ Mpc are consistent within the range of the 68% error. This result suggests that the systematic effects beyond the linear theory are small. The accuracy of the constraints on Ω_m and Ω_b increases by nearly a factor of 2 while the uncertainty of h is improved only marginally when the wider dynamical range is used. We obtain a relatively strong constraint on Ω_m without fixing the value of Ω_b because the constraint from the linear squashing effect in the anisotropic 2PCF is stronger than in the spherically averaged 2PCF. In addition, the best-fit value of Ω_m is in quite good agreement with an independent analysis of the LRGs by Percival et al. (2007b) using a power spectrum that yields $\Omega_m = 0.22 \pm 0.04$ with a dynamical range of $0.01 < k < 0.06h\mathrm{Mpc}^{-1}$. Our result also agrees with those from the CMB angular power spectra from *WMAP* (Spergel et al. 2007).

We note that the best-fit value of Ω_m is smaller (but not significantly so) than the result of E05, $\Omega_m = 0.273 \pm 0.025$. This is not surprising because the analytical methods differ from each other. The analysis in E05 is based on the spherically averaged 2PCF and uses information from smaller scales ($s < 40\ h^{-1}$ Mpc). They fix the baryon density parameter as $\Omega_b h^2 = 0.024$. We obtain a constraint of $\Omega_m h^2 = 0.123^{+0.048}_{-0.032}$ from our data when the parameter $\Omega_b h^2 = 0.024$ is fixed, as listed in Table 1 (see also Fig. 8). This result is consistent with the E05 result, $\Omega_m h^2 = 0.130 \pm 0.011$.

All the constraints obtained above are more conserva-

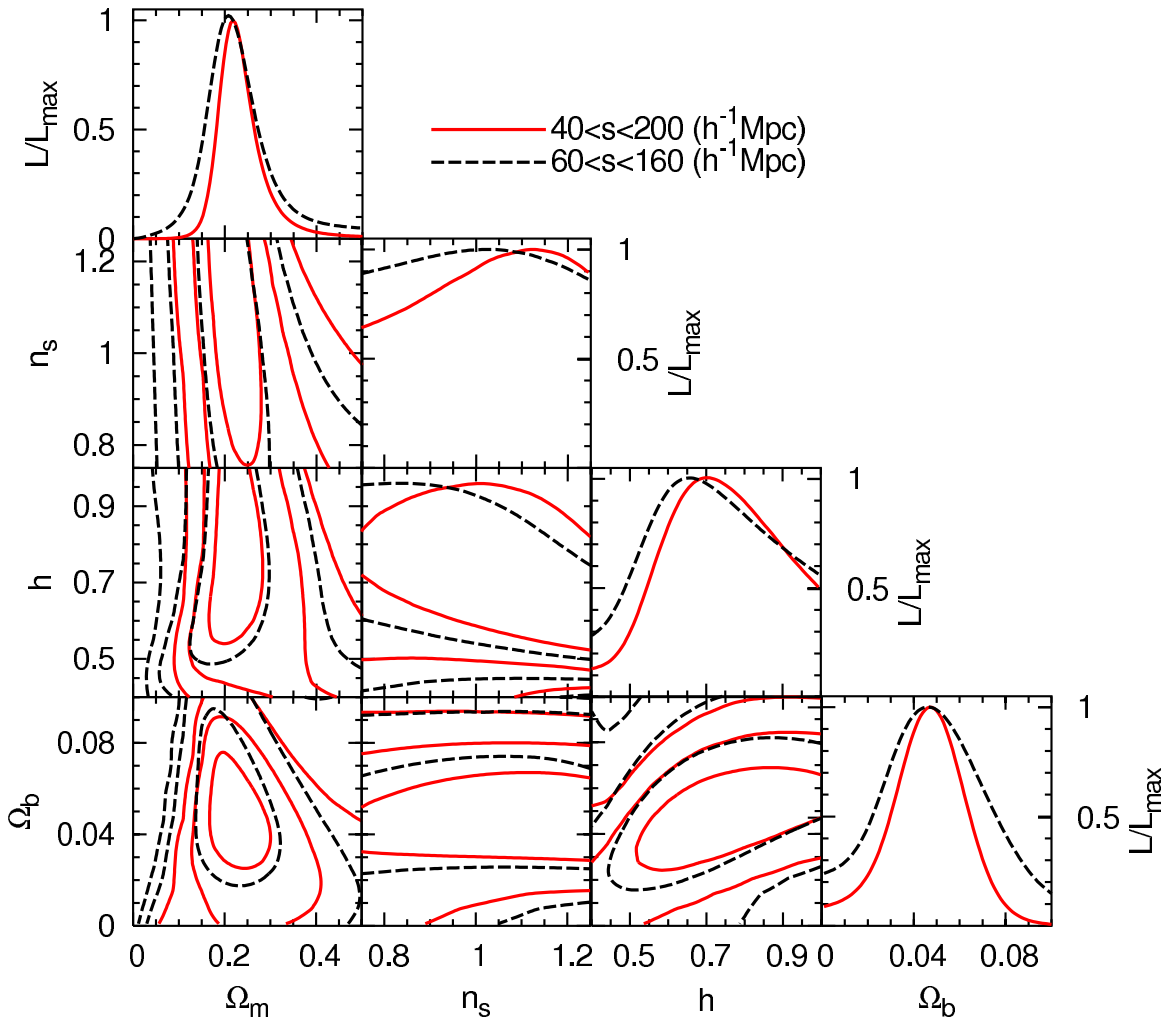

FIG. 7.— Likelihood contours for $(\Omega_m, \Omega_b, h, n_s)$, assuming a flat ΛCDM universe. The diagonal panels represent the likelihood functions for the four individual parameters with all the other parameters being marginalized over. The other panels show two-parameter constraints with the other parameters being marginalized, and each ellipse represents the constraint on the parameter space with 68%, 95%, and 99% from inward. As in Fig. 6, the solid (red) and dashed (black) contours are for $40 < s < 200\ h^{-1}$ Mpc and $60 < s < 160\ h^{-1}$ Mpc, respectively. The best-fit parameters for $40 < s < 200\ h^{-1}$ Mpc are $\Omega_m = 0.218$, $\Omega_b = 0.0473$, $h = 0.702$, and $n_s = 1.122$ and the minimum value of χ^2 is $\chi^2_{\rm min} = 421.5$ with 568 dof. For $60 < s < 160\ h^{-1}$ Mpc, the best-fit parameters are $\Omega_m = 0.208$, $\Omega_b = 0.0462$, $h = 0.656$, and $n_s = 1.030$ and $\chi^2_{\rm min} = 216.6$ with 324 dof.

TABLE 1
SUMMARY OF CONSTRAINTS ON COSMOLOGICAL PARAMETERS

	LRG only		LRG($40 < s < 200$)		
Parameter	$40 < s < 200$	$60 < s < 160$	+WMAP3	Marginalized	Fixed
$\Omega_{\rm m}$	$0.218^{+0.047}_{-0.037}$	$0.208^{+0.069}_{-0.055}$	$0.240^{+0.019}_{-0.025}$	$\Omega_{\rm b}, h, n_{\rm s}, \sigma_8, b$	w
$\Omega_{\rm b}$	$0.0473^{+0.0157}_{-0.0160}$	$0.0462^{+0.0253}_{-0.0208}$	$0.0414^{+0.0023}_{-0.0024}$	$\Omega_{\rm m}, h, n_{\rm s}, \sigma_8, b$	w
h	$0.702^{+0.187}_{-0.117}$	$0.656^{+0.220}_{-0.120}$	$0.718^{+0.023}_{-0.020}$	$\Omega_{\rm m}, \Omega_{\rm b}, n_{\rm s}, \sigma_8, b$	w
$n_{\rm s}$	$1.122^{+0.152}_{-0.183}$	$1.030^{+0.144}_{-0.189}$	$0.947^{+0.016}_{-0.015}$	$\Omega_{\rm m}, \Omega_{\rm b}, h, \sigma_8, b$	w
σ_8	$0.660^{+0.289}_{-0.216}$	$0.728^{+0.471}_{-0.359}$	$0.736^{+0.050}_{-0.062}$	$\Omega_{\rm m}, \Omega_{\rm b}, h, n_{\rm s}, b$	w
$\Omega_{\rm DE}$	$0.770^{+0.051}_{-0.040}$	$0.786^{+0.060}_{-0.061}$	$0.772^{+0.024}_{-0.033}$	$h, n_{\rm s}, w, \sigma_8, b$	$\Omega_{\rm b}h^2$
w	$-0.93^{+0.45}_{-0.35}$	$-1.07^{+0.49}_{-0.46}$	$-0.97^{+0.12}_{-0.11}$	$\Omega_{\rm DE}, h, n_{\rm s}, \sigma_8, b$	$\Omega_{\rm b}h^2$
$\Omega_{\rm m}$	$0.235^{+0.040}_{-0.037}$	—	—	h, σ_8, b	$\Omega_{\rm b}h^2$, $n_{\rm s}$, w
$\Omega_{\rm m}h^2$	$0.123^{+0.048}_{-0.032}$	—	—	h, σ_8, b	$\Omega_{\rm b}h^2$, $n_{\rm s}$, w

NOTE. — The comoving distance s is in units of h^{-1} Mpc. We assume $\Omega_{\rm b}h^2 = 0.024$, $w = -1$, and $n_{\rm s} = 0.98$ when they are fixed.

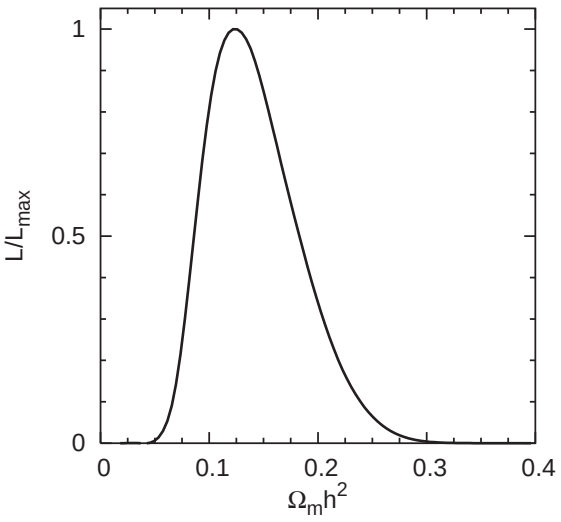

FIG. 8.— Likelihood function for a parameter $\Omega_m h^2$, fitted for the scale range of $40 < s < 200\ h^{-1}$ Mpc. The parameters h, σ_8, and b are marginalized over, and $\Omega_b h^2 = 0.024$ and $n_s = 0.98$ is fixed. For the best-fit parameter, $\chi^2_{\rm min} = 422.2$ with 570 dof.

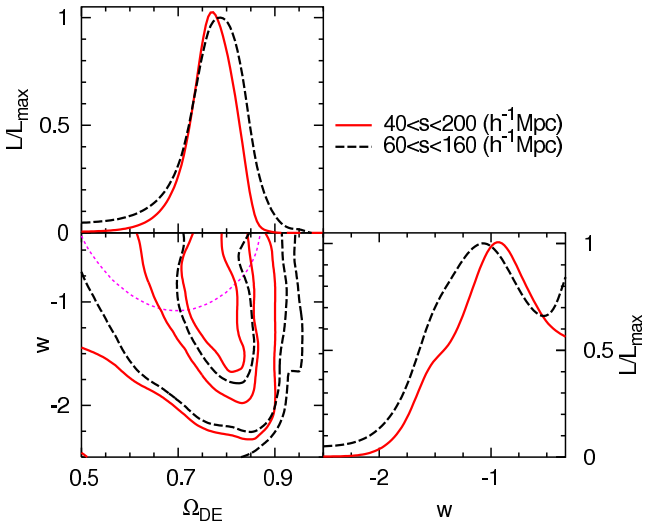

FIG. 9.— Dark energy constraints on $\Omega_{\rm DE}$ and w under the assumption of a flat universe and $\Omega_b h^2 = 0.024$. As in Fig. 7, the bottom left panel represents a two-parameter constraint, $\Omega_{\rm DE}$-w, with h, n_s, σ_8 and b marginalized over, and each ellipse represents the constraints on the parameter space with 68%, 95% and 99% from the inside. The solid (red) and dashed (black) contours are for $40 < s < 200$ and $60 < s < 160\ h^{-1}$ Mpc, respectively. The two diagonal panels represent likelihood functions with all the other four parameters marginalized over. The best-fit parameters are $\Omega_{\rm DE} = 0.770$, $w = -0.93$, where $\chi^2_{\rm min} = 421.2$ with 568 dof for $40 < s < 200\ h^{-1}$ Mpc, while $\Omega_{\rm DE} = 0.786$, $w = -1.07$ and $\chi^2_{\rm min} = 216.4$ with 324 dof. for $60 < s < 160\ h^{-1}$ Mpc. The dotted (magenta) contour in the bottom left panel shows the 68% CL when we smooth the oscillatory part of the transfer function and use it for the fit of $40 < s < 200\ h^{-1}$ Mpc.

tive than those in other work using the baryon acoustic oscillations because we neglect the small-scale data and all CMB information. For example, we obtain worse constraints on h than those on Ω_m. A possible reason for this is that discarding the small-scale data makes the constraints on $\Omega_m h^2$ degenerate along the direction of constant acoustic scales (see Fig. 8 of E05) and this direction is fairly parallel to the lines of constant Ω_m but intersects with the lines of constant h (Fig. 10 of E05).

5.4. *Dark energy constraint*

Constraining the dark energy is one of the most interesting applications of the anisotropic 2PCF. As described in § 4, we use the information from not only the overall shape of the 2PCF but also the geometrical distortion with baryon ridges to constrain the dark energy component. As Matsubara & Szalay (2002) indicated, the LRG sample is one of the best samples for probing the feature of dark energy among current redshift surveys. However, it is still difficult for the relatively low-z survey to constrain not only the value of w but also its evolution. In this subsection, we therefore assume w to be a constant not necessarily equal to -1 and fix $\Omega_b h^2 = 0.024$ because the baryon density is highly constrained by the analysis of the *WMAP* data (Spergel et al. 2007) and big bang nucleosynthesis (Burles et al. 2001). In Figure 9 we plot the joint likelihood functions of $\Omega_{\rm DE}$ and w and obtain $\Omega_{\rm DE} = 0.770^{+0.051}_{-0.040}$ and $w = -0.93^{+0.45}_{-0.35}$ for the fit to $40 < s < 200\ h^{-1}$ Mpc. All the other parameters but $\Omega_b h^2$ are marginalized over. Our constraints on dark energy parameters are listed in Table 1.

We also plot the likelihood function in the bottom left panel of Figure 9 where the no-wiggle power spectrum (Eisenstein & Hu 1998) is used to calculate the analytical formula for the anisotropic 2PCF. Because the dark energy parameter is constrained only from the overall shape of the 2PCF in this way and degenerates with the other parameters without information from the acoustic scale, we obtain a poorer fit to the data. Therefore, the overall shape is not a dominant effect in constraining the dark energy parameter, and the baryon ridges contribute as well.

5.5. *Combining with the WMAP results*

So far we have focused on parameter constraints using the LRG data only, which are very useful to check its result independently, while the obtained constraints are inevitably weaker than those we would obtain when other data sets are combined. In this subsection we consider the additional constraints using the CMB prior from the 3 year *WMAP* data (Spergel et al. 2007).

We consider two Markov chain Monte Carlo results of the *WMAP* data, $w = -1$ and constant w cosmologies (Tegmark et al. 2006). We find $\Omega_m = 0.240^{+0.019}_{-0.025}$, $\Omega_{\rm b} = 0.0414^{+0.0023}_{-0.0024}$, $h = 0.718^{+0.023}_{-0.020}$, $n_{\rm s} = 0.947^{+0.016}_{-0.015}$, $\sigma_8 = 0.736^{+0.050}_{-0.062}$, and $b = 2.15^{+0.28}_{-0.36}$ from the former chain, while $\Omega_{\rm DE} = 0.772^{+0.024}_{-0.033}$ and $w = -0.97^{+0.12}_{-0.11}$ from the latter. These constraints are also summarized in Table 1 and are in very good agreement with the previous studies for the joint constraints of the *WMAP* observation with the large-scale structure (e.g., Tegmark et al. 2006; Spergel et al. 2007). Although a pure LRG analysis cannot tightly constrain $\Omega_m h^2$ or h because of the limited range of separations, they are significantly improved by the prior on the CMB acoustic scale.

6. CONCLUSIONS

We have presented the 2PCF in redshift-space for the SDSS Luminous Red Galaxy sample considering the anisotropy in 2D redshift space. In particular, we have focused on the distorted features of the 2PCF in redshift-space from both peculiar velocities of galaxies and geometrical effect. The distorted features of the Kaiser and

finger-of-God effects were clearly detected. The baryon ridges, which are the baryonic acoustic features in the anisotropic 2PCF, are a nearly spherical object in comoving space. We found indications of baryon ridges in the measured 2PCF. Beyond qualitative comparison between data and theory, evaluation of the covariance matrix is needed for cosmological parameter estimation. We constructed the matrix by generating mock samples using the second-order Lagrangian perturbation theory with an artificial biasing scheme. We have constrained the cosmological parameters by comparing the observed 2PCF with linear theory.

We have obtained constraints on fundamental cosmological parameters, $\Omega_m = 0.218^{+0.047}_{-0.037}$, $\Omega_b = 0.0473^{+0.0157}_{-0.0160}$, $h = 0.702^{+0.187}_{-0.117}$, and $n_s = 1.122^{+0.152}_{-0.183}$ when we have used the data of $40 < s < 200\ h^{-1}$ Mpc. The constraint on Ω_m was better mainly because of the clear detection of the Kaiser effect, which directly depends on Ω_m through β. We have also obtained the constraints on the dark energy as $\Omega_{\rm DE} = 0.770^{+0.051}_{-0.040}$ and $w = -0.93^{+0.45}_{-0.35}$ when we fix $\Omega_b h^2 = 0.024$ and the other parameters, h, $n_{\rm s}$, σ_8, and b are marginalized over. These constraints are mainly due to the overall shape of the anisotropic 2PCF and the information from geometrical distortions including the scale of the baryon ridge. We have demonstrated that a pure LRG analysis can constrain w by considering the anisotropy of the structure accurately. As for the parameters related to the clustering amplitude, we have obtained $\sigma_8 = 0.66^{+0.289}_{-0.216}$ and $b = 1.55^{+1.42}_{-0.75}$. While these two parameters are strongly coupled, the degeneracy was alleviated from anisotropy of the 2PCF through the redshift distortion factor, β. In addition, stronger constraints on the cosmological parameters above were obtained by the CMB prior from the 3 year *WMAP* results. All the constraints summarized above agree with the previous studies in literature.

The current analysis can be improved by considering two issues below. The first issue is theoretical improvement accounting for the nonlinearity of the gravitational evolution, the redshift distortions and the galaxy biasing. Although the baryonic signature emerges on very large scales, the width of the baryon peak in the 2PCF is an order of 10 Mpc. The nonlinearities nontrivially affect such a feature. In fact, such effects have already been investigated using N-body simulations, higher-order perturbation theories, and renormalization perturbation theory (Meiksin et al. 1999; Seo & Eisenstein 2005; Springel et al. 2005; Jeong & Komatsu 2006; Crocce & Scoccimarro 2007; Nishimichi et al. 2008; Matsubara 2007). The degradation of the acoustic signature was well modeled; it was shown that the acoustic peak of the linear density field in the 2PCF can be reconstructed (Eisenstein et al. 2007a,b). In addition, the overall shape of the redshift-space 2PCF is also affected by nonlinear dynamics (Scoccimarro 2004). According to his result, the redshift-space 2PCF for pairs parallel to the line of sight in a random Gaussian field deviates from the prediction of standard linear theory even on fairly large scales. In this work we do not use the data along the line of sight; however, we shall include these issues in the future analysis. The theoretical and numerical studies also suggest that the biasing is potentially scale dependent even on large scales (e.g., Schulz & White 2006; Smith et al. 2007; Coles & Erdoğdu 2007), which poses a serious problem for estimating cosmological parameters from galaxy surveys (Blanton et al. 2006; Percival et al. 2007b; Sánchez & Cole 2008).

The second issue is the calculation of the covariance matrix for the measured 2PCF. As described in § 3.2, we have constructed a covariance matrix by the second-order perturbation theory. Using N-body simulations which fully include nonlinearity provides better estimation of the covariance matrix. However, this approach is too computationally expensive to produce a large number of independent realizations. The approximation by the second-order perturbation theory is valid on scales which we consider in this work. However, in order to utilize the information at smaller scales for more accurate cosmological parameter estimation, we must estimate the nonlinearities more accurately using N-body simulations or more sophisticated methods such as a halo occupation model from the second-order Lagrangian perturbation theory (e.g., Scoccimarro & Sheth 2002).

The most important point of our analysis is that we directly include anisotropies of the structure. The baryonic features enable to divide the effect of the redshift distortions into dynamical and geometrical components. The anisotropy due to the geometric distortion, in particular, contributes to better estimation of the equation-of-state parameter for the dark energy. Various methods using the scale of the oscillations as a standard ruler have been considered for both the power spectrum and the 2PCF (Eisenstein & Hu 1998; Blake & Glazebrook 2003; Hu & Haiman 2003; Seo & Eisenstein 2003; Matsubara 2004; Glazebrook & Blake 2005). This work is the first application of the anisotropy in the 2PCF with baryon acoustic features to observational data, which was proposed by Matsubara (2004). Direct measurement of the growth function from the Kaiser's effect and the two-dimensional acoustic scales which depend on $D_A(z)$ and $H(z)$ is also an attractive challenge of the analysis using the anisotropic 2PCF, so these topics will be definitely pursued in future work with an improved LRG sample.

The baryonic signature from the redshift range of SDSS LRGs is not strong, because their number density is relatively small and nonlinear effects weaken the baryonic feature. There are many plans for constraining the dark energy by future wide-field, deep galaxy surveys: the Fiber Multiobject Spectrograph (FMOS; Kimura et al. 2003), Wide-Field Multiobject Spectrograph (WFMOS; Glazebrook & Blake 2005; Bassett et al. 2005), Baryon Oscillation Probe (BOP; Glazebrook et al. 2005), and the Hobby-Eberly Dark Energy Experiment (HETDEX; Hill et al. 2004), and so on. When the baryonic signature is detected with high accuracy from future redshift surveys, the analysis of the anisotropic 2PCF as in this work will be an important ingredient for stringently constraining properties of the dark energy.

We acknowledge helpful discussions with Naoshi Sugiyama, Roman Scoccimarro, and Kazuhiro Yahata. We also thank the anonymous referee for useful comments. This work is supported in part by Grand-in-Aid for Scientific Research on Priority Areas, No. 467, Probing the Dark Energy through an Extremely Wide and Deep Survey with the Subaru Telescope, and by

the Mitsubishi Foundation. T. M. acknowledges support from the Ministry of Education, Culture, Sports, and Technology (MEXT), and Grant-in-Aid for Scientific Research (No. 18540260). I. K. acknowledges support from the MEXT, and a Grant-in-Aid for Encouragement of Young Scientists (No. 17740139). C. H. acknowledges support from a JSPS (Japan Society for the Promotion of Science) fellowship. C. H. also acknowledges the support from the Particle Physics and Astronomy Research Council grant PP/C501692/1. Numerical calculations are performed by a parallel computing system at Nagoya University. Funding for the SDSS and SDSS-II has been provided by the Alfred P. Sloan Foundation, the Participating Institutions, the National Aeronautics and Space Administration, the Japanese Monbukagakusho, the Max Planck Society, and the Higher Education Funding Council for England. The SDSS Web Site is http://www.sdss.org/.

The SDSS is managed by the Astrophysical Research Consortium for the Participating Institutions. The Participating Institutions are the American Museum of Natural History, Astrophysical Institute Potsdam, University of Basel, University of Cambridge, Case Western Reserve University, University of Chicago, Drexel University, Fermilab, the Institute for Advanced Study, the Japan Participation Group, Johns Hopkins University, the Joint Institute for Nuclear Astrophysics, the Kavli Institute for Particle Astrophysics and Cosmology, the Korean Scientist Group, the Chinese Academy of Sciences (LAMOST), Los Alamos National Laboratory, the Max Planck Institute for Astronomy (MPIA), the Max-Planck-Institute for Astrophysics (MPA), New Mexico State University, Ohio State University, University of Pittsburgh, University of Portsmouth, Princeton University, the United States Naval Observatory, and the University of Washington.

REFERENCES

Abazajian, K., et al. 2004, AJ, 128, 502
Alcock, C., & Paczyński, B. 1979, Nature, 281,358
Ballinger, W. E., Peacock, J. A., & Heavens, A. F. 1996, MNRAS, 282, 877
Bassett, B. A., Nichol, B., & Eisenstein, D. J., 2005, Astron. Geophys., 46, 26
Bernstein, G. M. 1994, ApJ, 424, 569
Blake, C., & Glazebrook, K., 2003, ApJ, 594, 665
Blake, C., Collister, A., Bridle, S., & Lahav, O., 2006, MNRAS, 374, 1527
Blanton, M. R., Eisenstein, D. J., Hogg, D. W., & Zehavi, I. 2005, ApJ, 645, 977
Blanton, M. R., Lin, H., Lupton, R. H., Maley, F. M., Young, N., Zehavi, I., & Loveday, J. 2003a, AJ, 125, 2276
Blanton, M. R., et al. 2003b, AJ, 125, 2348
Blanton, M. R., et al. 2005, AJ, 129, 2562
Burles, S., Nollett, K. M., & Turner, M. S. 2001 Phys. Rev. D, 63, 3512
Cole, S., et al. 2005, MNRAS, 362, 505
Coles, P., & Erdoğdu, P. 2007, J. Cosmology Astropart. Phys., 10, 7
Colless, M., et al. 2001, MNRAS, 328, 1039
Crocce, M., Pueblas, S., & Scoccimarro, R. 2006, MNRAS, 373, 369
Crocce, M., & Scoccimarro, R. 2007, Phys. Rev. D, 77, 023533
da Ângela, J., Outram, P. J., Shanks, T., Boyle, B. J., Croom, S. M., Loaring, N. S., Miller, L., & Smith, R. J. 2005, MNRAS, 360, 1040
Davis, M., & Peebles, P. J. E. 1983, ApJ, 267, 465
Eisenstein, D. J., & Hu, W. 1998, ApJ, 496, 605
Eisenstein, D. J., Hu, W., & Tegmark, M. 1999, ApJ, 518, 2
Eisenstein, D. J., Seo, H., Sirko, E., & Spergel, D. N. 2007a, ApJ, 664, 675
Eisenstein, D. J., Seo, H., & White, M. 2007b, ApJ, 664, 660
Eisenstein, D. J., et al. 2001, AJ, 122, 2267
Eisenstein, D. J., et al. 2005, ApJ, 633, 560 (E05)
Feldman, H. A., Kaiser, N., & Peacock, J. A. 1994, ApJ, 426, 23
Fisher, K. B., Davis, M., Strauss, M. A., Yahil, A., & Huchra, J. 1994, MNRAS, 266, 50
Fukugita, M., Ichikawa, T., Gunn, J. E., Doi, M., Shimasaku, K., & Schneider, D. P. 1996, AJ, 111, 1748
Glazebrook, K., & Blake, C. 2005, ApJ, 631, 1
Glazebrook, K., et al. 2005, preprint (astro-ph/0507457)
Gunn, J. E., et al. 1998, AJ, 116, 3040
Gunn, J. E., et al. 2006, AJ, 131, 2332
Hamilton, A. J. S. 1992 ApJ, 385, 5
Hawkins, E., et al. 2003, MNRAS, 346, 78
Hill, G. J., Gebhardt, t., Komatsu, E., & MacQueen, P. J. 2004, in AIP Conf. Proc., 743, The New Cosmology: Conference on Strings and Cosmology (New York: AIP), 224
Hogg, D. W., Finkbeiner, D. P., Schlegel, D. J., & Gunn, J. E. 2001, AJ, 122, 2129
Hoyle, F., Outram, P. J., Shanks, T., Boyle, B. J., Croom, S. M., & Smith, R. J. 2002, MNRAS, 332, 311
Hu, W., & Haiman, Z., 2003, Phys. Rev. D, 68, 063004
Hütsi, G., 2006a, A&A, 449, 891
Hütsi, G., 2006b, A&A, 459, 375
Ivezić, Ž., et al. 2004, AN, 325, 583
Jeong, D., & Komatsu, E. 2006, ApJ, 651, 619
Kaiser, N. 1987, MNRAS, 227, 1
Kimura, M., et al. 2003, Proc. SPIE, 4841, 974
Landy, S. D., & Szalay, A. D. 1993, ApJ, 412, 64
Lupton, R. H 1993, Statistics in Theory and Practice (Princeton: Princeton Univ. Press)
Lupton, R. H., Gunn, J. E., Ivezic, Z., Knapp, G. R., Kent, S., & Yasuda, N. 2001, in ASP Conf. Ser. 238, Astronomical Data Analysis Software and Systems X. ed. F. R. Harnden, Jr., F. A. Primini, and H. E. Payne (san Francisco: Astr. Spc. Pac.), 269
Matsubara, T. 2000, ApJ, 535, 1
Matsubara, T. 2004, ApJ, 615, 573
Matsubara, T. 2007, Phys. Rev. D, submitted (arXiv:0711.2521)
Matsubara, T., & Suto, Y. 1996, ApJ, 470, 1
Matsubara, T., & Szalay, A. S. 2001, ApJ, 556, 67
Matsubara, T., & Szalay, A. S. 2002, ApJ, 574, 1
Meiksin, A., White, M., & Peacock, J. A. 1999, MNRAS, 304, 851
Nishimichi, T., et al. 2008, PASJ, in press (arXiv:0705.1589)
Outram, P. J., Shanks, T., Boyle, B. J., Croom, S. M., Hoyle, F., Loaring, N. S., Miller, L., Smith, R. J. 2004, MNRAS, 348, 745
Padmanabhan, N., et al. 2007, MNRAS, 378, 852
Peacock, J. A., et al. 2001, Nature, 410, 169
Peebles, P. J. E. 1980, The Large-Scale Structure of the Universe (Princeton: Princeton Univ. Press)
Percival. W. J., et al. 2007a, ApJ, 657, 51
Percival. W. J., et al. 2007b, ApJ, 657, 645
Perlmutter, S., et al. 1999, ApJ, 517, 565
Pier, J. R., Munn, J. A., Hindsley, R. B., Hennessy, G. S., Kent, S. M., Lupton, R. H., & Ivezić, Ž. 2003, AJ, 125, 1559
Pope, A. C., & Szapudi, I. 2007, MNRAS, submitted (arXiv:0711.2509)
Riess, A. G., et al. 1998, AJ, 116, 1009
Ross, N. P., et al. 2007, MNRAS, 381, 573
Sánchez, A. G., & Cole, S. 2008, MNRAS, in press (arXiv:0708.1517)
Schulz, A. E., & White, M. 2006, Astropart. Phys., 25, 172
Scoccimarro, R., 2004, Phys. Rev. D, 70, 083007
Scoccimarro, R., & Sheth, R. K. 2002, MNRAS, 329, 629
Seljak, U., & Zaldarriaga, M. 1996, ApJ, 496, 437
Seo, H., & Eisenstein, D. J. 2003, ApJ, 598, 720
Seo, H., & Eisenstein, D. J. 2005, ApJ, 633, 575
Seo, H., & Eisenstein, D. J. 2007, ApJ, 665, 14
Smith, J. A., et al. 2002, AJ, 123, 2121
Smith, R. E., Scoccimarro, R., & Sheth, R. K. 2007, Phys. Rev. D, 75, 063512
Spergel, D. N., et al. 2007, ApJS, 170, 377
Springel, V., et al. 2005, Nature, 435, 629

Stoughton, D. G., et al. 2002, AJ, 123, 485
Szalay, A. S., Matsubara, T., & Landy, S. D. 1998, ApJ, 498, 1
Tegmark, M., et al. 2006, Phys. Rev. D, 74, 123507
Tucker, D., et al. 2006, Astron. Nachr., 327, 821
Yahata, K., et al. 2005, PASJ, 57, 529
Yamamoto, K., & Suto, Y. 1999, ApJ, 517, 1
York, D. G., et al. 2000, AJ, 120, 1579
Zehavi, I., et al. 2005, ApJ, 621, 22